DSE-8033-1/3

CADMIUM SULFIDE/COPPER SULFIDE HETEROJUNCTION CELL RESEARCH

Technical Progress Report for September 1—November 30, 1979

By
W. W. Anderson
A. D. Jonath

February 1980

Work Performed Under Contract No. EG-77-C-01-4042

Lockheed Missiles & Space Company, Inc.
Palo Alto Research Laboratory
Palo Alto, California

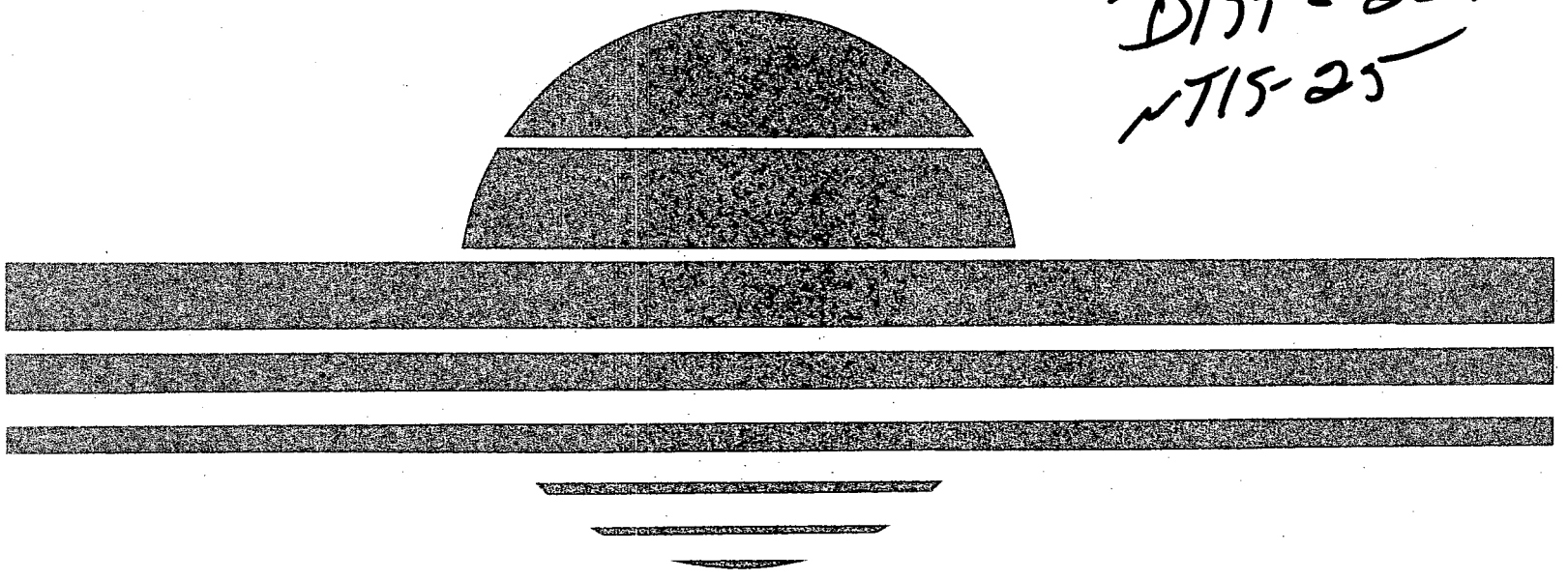

U.S. Department of Energy

Solar Energy

DISCLAIMER

Available from the National Technical Information Service, U. S. Department of Commerce, Springfield, Virginia 22161.

Price: Paper Copy $5.00
Microfiche $3.50

DISCLAIMER

LMSC-D682102

DSE-8033-1/3
Distribution Category UC-63c

CADMIUM SULFIDE/COPPER SULFIDE HETEROJUNCTION CELL RESEARCH

Technical Progress Report
For Period Sep 1, 1979 - Nov 30, 1979

W. W. Anderson
A. D. Jonath

February 1980

Work Performed Under Contract XJ-9-8033-1

LOCKHEED MISSILES & SPACE COMPANY, INC.
Palo Alto Research Laboratory
3251 Hanover St.
Palo Alto, CA 94304

ABSTRACT

Several all sputter deposited Cu_2S/CdS cells have been prepared to date with $J_{SC} \approx 3$ mA/cm^2 under simulated AM1 illumination. The best AM1 conversion efficiency obtained is 0.6%. This is shown to be typical of sputtered CdS in Cu_2S/CdS cells investigated to date. The sputtered Cu_2S appears to be satisfactory for solar cell applications.

Presented evidence indicates that the poor conversion efficiency is due to a low-junction electric field intensity on the CdS side of the heterojunction. A multilayer CdS structure has been developed which may allow the tailoring of the junction electric field intensity to a selected high value to obtain high-junction collection efficiency.

Other areas of cell development advances included:

- Determination of effect of Cu cones in Cu_2S on Cu_2S/CdS cell performance
- Solution of CdS pinhole problem
- Open circuit voltage improvement by heat treatment.

CONTENTS

ILLUSTRATIONS

TABLES

Section 1
INTRODUCTION

The program objective is to investigate and evaluate the application of cylindrical-post-magnetron reactive sputtering to the production of solar-cell quality thin films of CdS/Cu_2S for large-scale terrestrial photovoltaic energy conversion.

All sputter-deposited CdS/Cu_2S solar cell structures have been prepared. Deposition parameters are sufficiently well understood and controlled so that reproducible thin film material and device properties can be obtained from run to run. The I-V characteristic of the best cell prepared to date is shown in Fig. 1. In Table 1 the salient performance characteristics are compared with the optimum computed performance for this device. Computations are from Reference 1 with V_{oc} for pure CdS and $L_n = 0.1\ \mu m$. It is obvious that the major deficit of the present device is in the short circuit current. The fill factor is the second most serious problem.

Several cells have been prepared to date with $J_{sc} \approx 3\ mA/cm^2$ under simulated AM 1 illumination as listed in Table 2. Cells No. 653 and 654 were prepared by cyclically sputtering Cd in H_2S/Ar and in pure Ar. Cells No. 824, 825, 917, and 920 were prepared by depositing $0.5\ \mu m$ of undoped CdS onto 4 to 7 μm of CdS:In. Both sets of cells had wide depletion layers after heat treatment, even under AM 1 illumination, W(AM1, $V = 0) \approx 2\ \mu m$. Using Rothwarf's theory of field-aided collection across the heterojunction interface (Ref. 2), we find the poor short circuit current to be primarily due to the low collection field in the CdS. Other current loss mechanisms such as grid shadowing and surface reflectance have been quantified and found to be small compared to the interface recombination.

The low fill factor may also be shown to depend on the interface recombination process in the cells. The open circuit voltage will increase with improved short circuit current

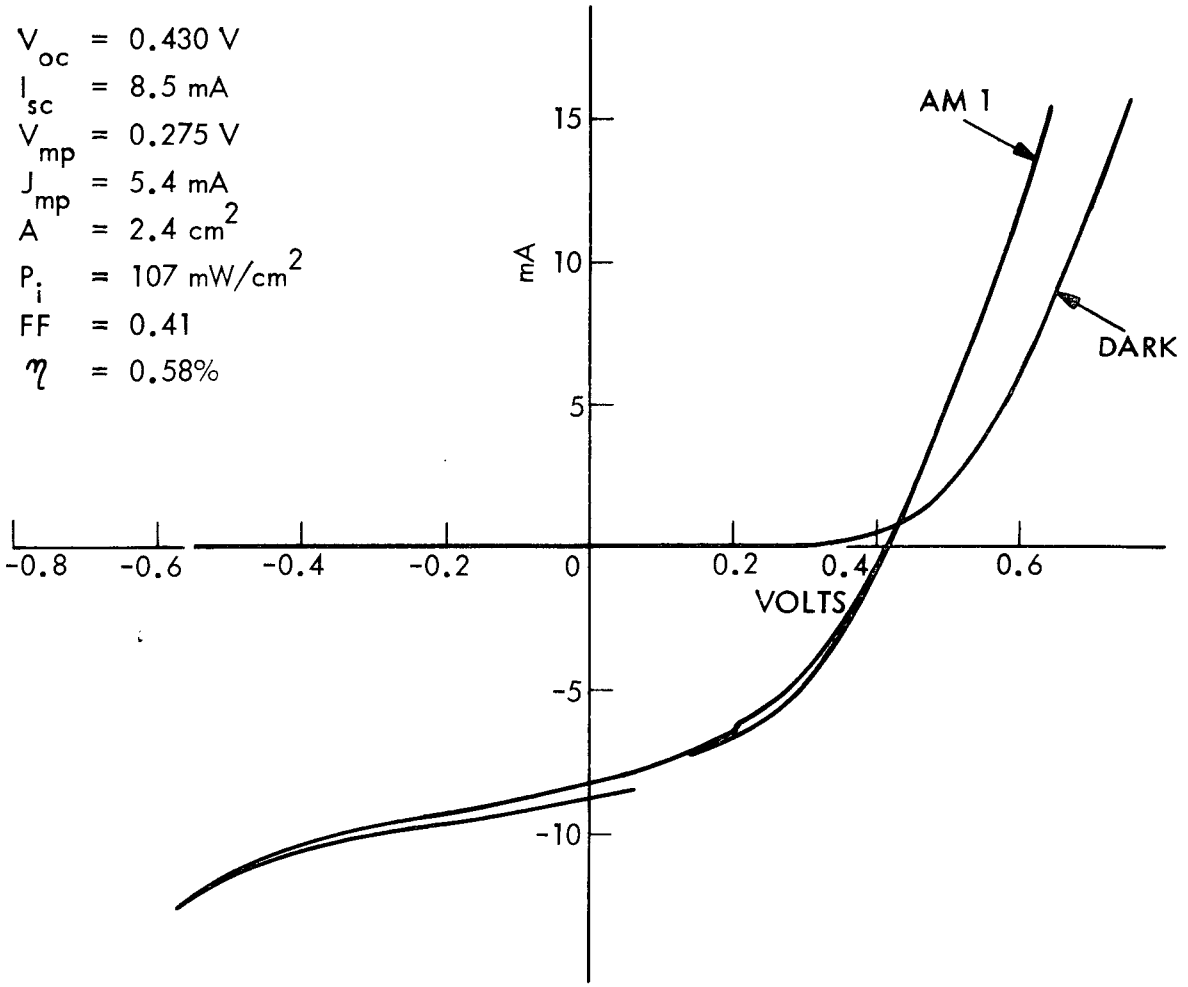

Fig. 1 CdS/Cu_2S Solar Cell No. 653 Characteristics

Table 1

COMPARISON OF DEVICE CHARACTERISTICS OBTAINED TO COMPUTED OPTIMUM (REF. 1)

Parameter	Measured	Optimum	Ratio
J_{SC} (mA/cm^2)	3.4	15.5	0.22
FF	0.41	0.8	0.51
V_{oc} (V)	0.43	0.54	0.80
η (%)	0.58	6.5	0.09

Table 2

SHORT CIRCUIT CURRENT

Cell No.	Isc (mA)	A (cm^2)	Jsc (mA/cm^2)
653	8.5	2.4	3.5
654	10	3.75	2.7
824	8.0	2.18	3.7
825	5.2	2.43	2.14
917	8.8	3.58	2.46
920	10	3.76	2.66

However, there is an additional voltage drop across the present junctions which has the characteristics of a TFL space charge limited current flow (Ref. 3).

The primary effort for the remainder of the present program is to use the unique capabilities of the sputter process to tailor the interfacial junction field to a high value ($E_o \gtrsim 8 \times 10^4$ V/cm). In conventional CdS film processing (vacuum evaporation or spray pyrolysis), a stoichiometric excess of Cd is compensated by Cu interdiffusion during cell heat treatment. The Cu compensated region then exhibits a trapping mode photoconductivity which collapses the space charge region, resulting in an interfacial collection field of the order 4 to 8 $\times 10^4$V/cm. During sputter deposition, it is difficult to obtain significant deviations from stoichiometry. Techniques for stoichiometry control unique to the reactive sputtering process as well as graded doping techniques are currently under investigation. By graded doping, $E_o \approx 4 \times 10^4$ V/cm has been obtained in an as-deposited device structure. However, E_o then dropped during heat treatment required to activate the cell.

Other significant activities in the present reporting period include:

- Consistent attainment of 100% area integrity of thin film devices as evidenced by response to individual grid lines
- Attainment of truly planar device structures as verified by observation of interference fringes in both CdS and Cu_2S layers of cell
- Application of specialized diagnostic techniques to CdS/Cu_2S device structures including:
  - (a) Temperature-dependent I-V analysis of SCL-like current in Cu_2S/CdS junctions
  - (b) Junction profiling via C-V analysis, both with and without AM 1 illumination
  - (c) Spectral response analysis, both with and without AM 1 illumination

Specific diagnostic procedures were targeted to elucidate specific material or device parameters at each stage of the sputter deposition process development. This serial

approach to a novel technology development has resulted in slow but steady progress toward the program goal. It has also allowed the isolation and solution of individual deposition process problems as they arose without a concomitant loss of control of interrelated material or device parameters.

Section 2

INDIVIDUAL LAYER CHARACTERIZATION

2.1 Cu_2S CHARACTERIZATION

It has been generally accepted that chalcocite is the desired Cu_xS phase for solar cell applications (Refs. 4 and 5). Refined analysis of the Cu_2S/CdS cell suggests an optimum departure of Cu_xS from stoichiometry ($x = 2$) to $x = 1.9995$ (Ref. 6) which is within the chalcocite phase existence region (Ref. 7). Early in this program we established the phase/H_2S pressure/substrate temperature relationship for Cu_xS deposited onto glass substrates (Ref. 8). Three important results were derived from this work:

- A "resistivity gap" exists between the chalcocite phase and the lower Cu content phases. High room temperature resistivity ($\rho \sim 10$ to 10^2 Ω-cm) is adequate to identify the predominence of the chalcocite phase
- Excess Cu precipitates out in the form of Cu nodules or cones. The presence of Cu nodules is sufficient but not necessary to identify a film as predominantly chalcocite
- The optical absorption characteristics of Cu_xS films are accurately described by the empirical relations determined from single crystal studies (Refs. 8, 9, 10)

This early work was partially repeated to verify that similar deposition parameter/Cu_xS phase relations existed when Cu_xS was sputtered onto a CdS film. It was found that similar relations do exist and that chalcocite is readily obtained. New information on the importance of chamber wall effects specific to the Cu_2S deposition process was obtained from this second study (Refs. 11, 12).

A significant finding of the Cu_2S deposition onto CdS study was:

- Cu cones do not result in excessive cell shunt conductance

An early result of studies on Clevite cells showed that Cu nodule growth down grain boundaries resulted in cell degradation (Ref. 5). The growth characteristic of Cu nodules in sputter-deposited Cu_2S is up from the CdS top surface through the Cu_2S film as shown in the SEM photo of Fig. 2a. The depth of the hole left where the Cu cones have "fallen out" is 0.15 μm, i.e., the thickness of the Cu_2S layer only. Some surface texture results when a thick CdS film is grown as shown in Fig. 2b, but the Cu cone formation is essentially the same as on a smooth surface. Figure 2b is the top surface of Cell No. 803. There was no evidence of shunting conductance due to the high density of Cu cones. The very dense CdS film produced by sputtering precludes Cu nodule growth down to the metallic substrate. (See Fig. 3.)

A definite deleterious effect of Cu cone formation is reduction of a portion of the active surface of the cell, resulting in a reduced short-circuit current. Cell No. 824 had a fractional area coverage of only 0.36% while Cell No. 920 had a fractional area coverage of 19.5% due to Cu cones.) Earlier experiments on Cu_2S over glass substrates showed a constant "effective" absorption constant for $\lambda > 1.1$ μm which was determined by the fractional area covered by Cu cones (Figure 13 of Ref. 8).

A possible deleterious effect is reduction of open circuit voltage. From Fig. 2a we see that the Cu may physically contact the CdS surface. Cu forms a Schottky barrier to CdS with $\phi_B = 0.35$ volts on an atomically clean CdS surface (Refs. 13, 14), but with $\phi_B = 0.7$ volts on a slightly oxidized surface (Ref. 14). For $\phi_B = 0.35$ volts, a reduced open circuit voltage may result due to forward biasing of the Cu/CdS Schottky barrier regions.

The Cu cone density on Cells No. 824 and 825 was too insignificant to effect either the short-circuit current or the open circuit voltage. The recent Cu_2S deposition study has shown that, with a heated CdS substrate ($T_S \approx 150$ C):

- Increasing H_2S partial pressure during deposition reduces the Cu cone density (Ref. 12).

The initial photo-electronic interaction in the Cu_2S/CdS cell takes place in the Cu_2S layer of the cell. Optical absorption and cell shortcurrent spectral response measure-

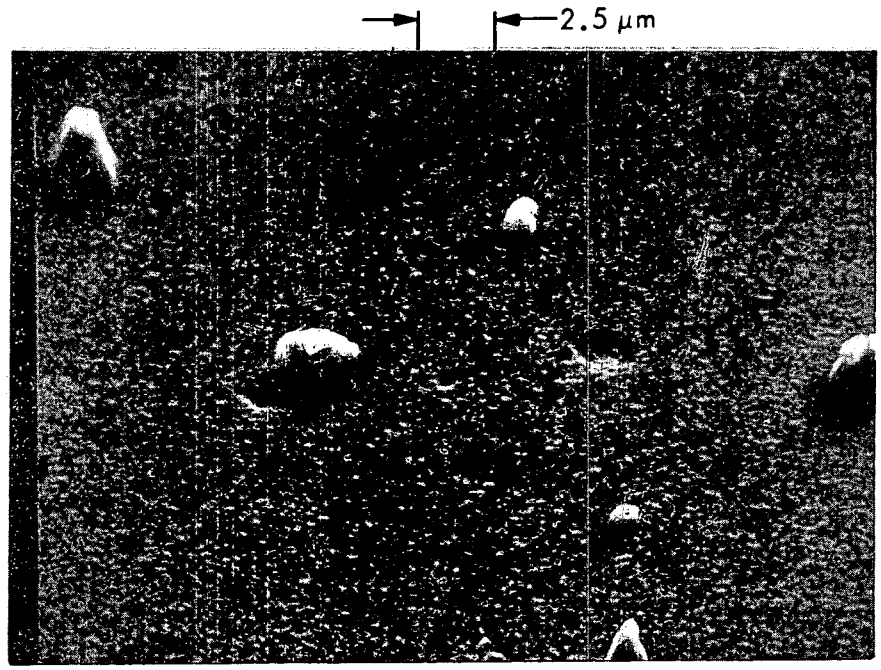

a. Cu Cone formation in Cu_2S grown over 0.5-μm thick CdS

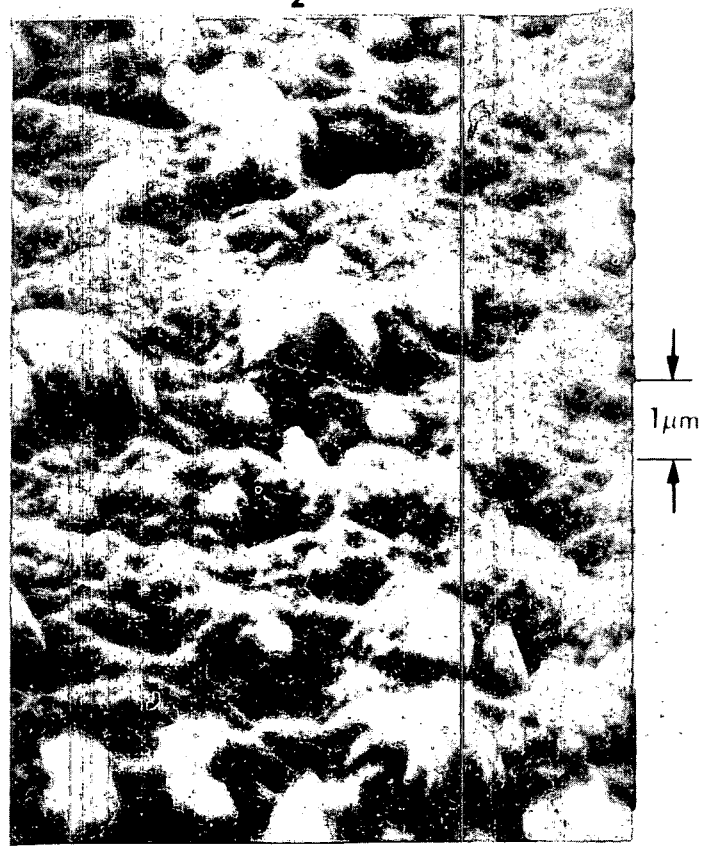

b. Cu Cone formation in Cu_2S grown over 7-μm thick CdS

Fig. 2 Copper Nodule or Cone Growth in Cu_2S Deposited on CdS

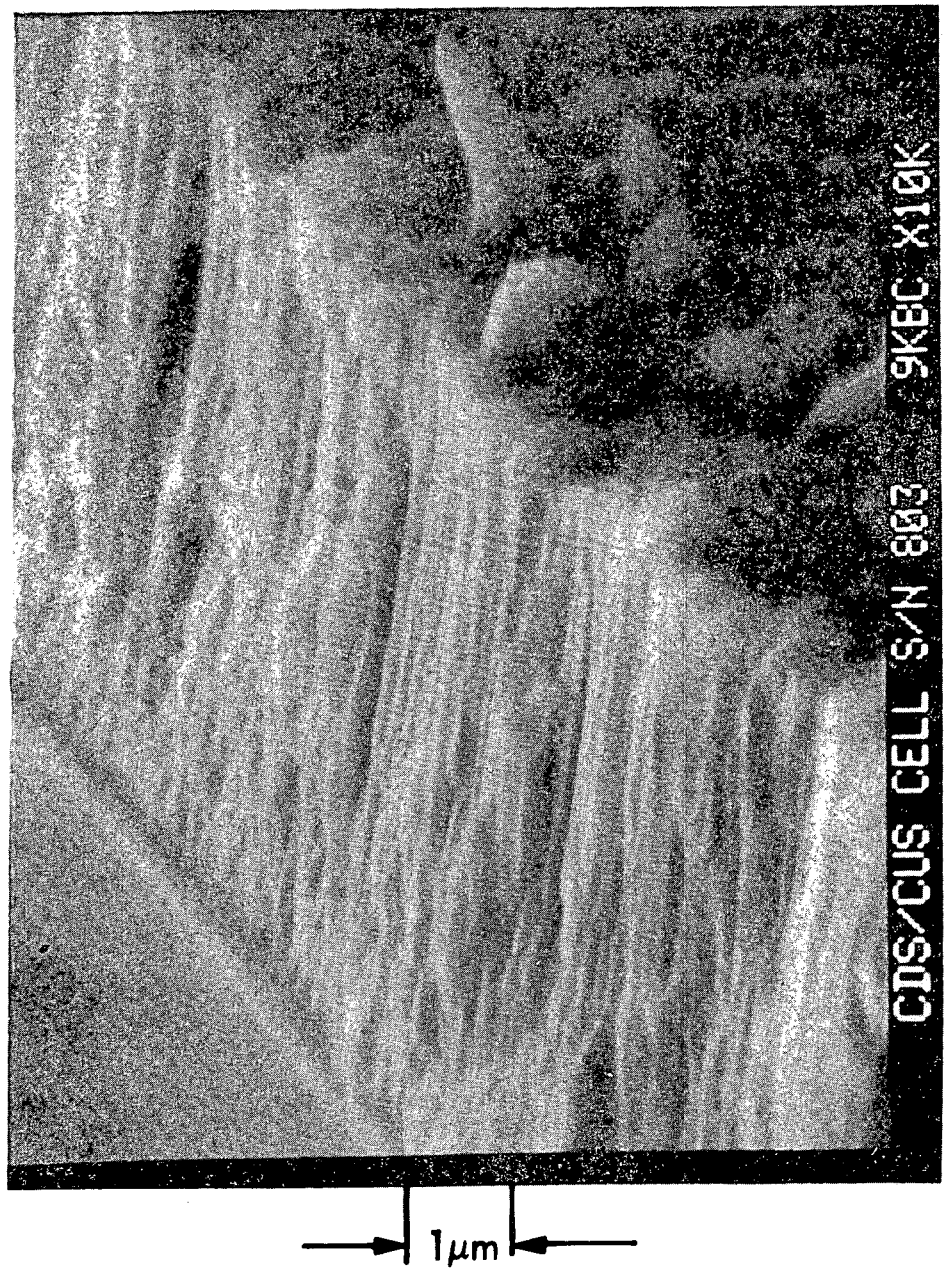

Fig. 3 SEM Cross Section of Cu_2S/CdS/CdS:In Solar Cell Structure

ments indicate that sputter-deposited Cu_2S has optical characteristics close to conventional topotaxially grown Cu_2S. Cell photocurrent spectral response measurements also indicate minority carrier (electron) diffusion lengths comparable to those of conventional cells ($L_n \sim .1 - .3\ \mu m$). Analysis indicates that present device limitation occurs at the Cu_2S/CdS interface. Therefore, the present status of sputter-deposited Cu_2S may be considered acceptable while the CdS and interface are investigated. When satisfactory junction collection efficiency is obtained, the Cu_2S study can be resumed to maximize V_{oc}, minimize series resistance, maximize minority carrier diffusion length, and minimize surface recombination velocity.

2.2 THIN FILM INTEGRITY

Cu_2S/CdS composite films are deposited over 5 cm^2 of a 6.5 cm^2 Nb-coated glass substrate. An array of 31 Au fine line grids is then deposited over 4.1 cm^2 of the Cu_2S/CdS area. (Note that all of the cell areas listed in Table 2 are less than total gridded area. The most common reason for reduced active area was associated with excessive Au grid width due to lifting of the grid deposition mask. Opaque Au areas were simply removed by scribing of cell surface.)

Individual Au grid lines are probed for evaluation of device characteristics before an interconnect bus bar is deposited. When low leakage diode characteristics are observed, the Cu_2S resistivity may be obtained from the resistance measured between two adjacent Au grid lines.

Three distinct cases are typically observed from an individual Au grid line evaluation:

- Isolated poor diode characteristics that strongly influence adjacent Au grid line diode characteristics; this immediately indicates a low resistivity Cu_2S phase (Fig. 4a)
- Isolated poor diode characteristics with no discernible effect on adjacent Au grid line diode characteristics; this immediately indicates a high resistivity (chalcocite) Cu_2S phase (Fig. 5a)

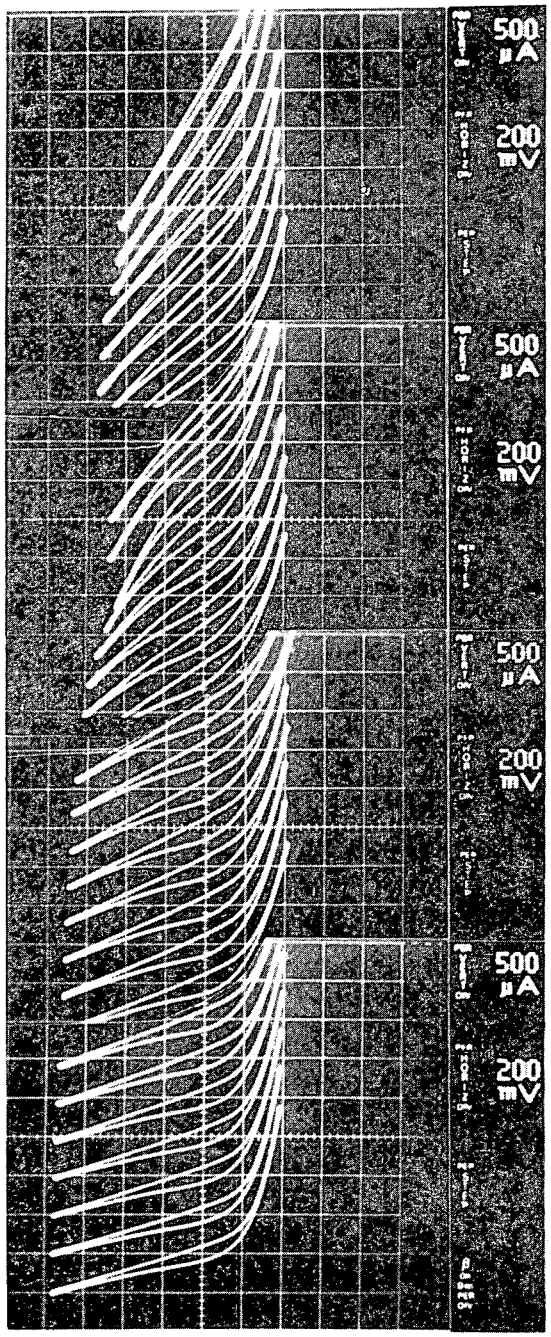

a. As deposited.

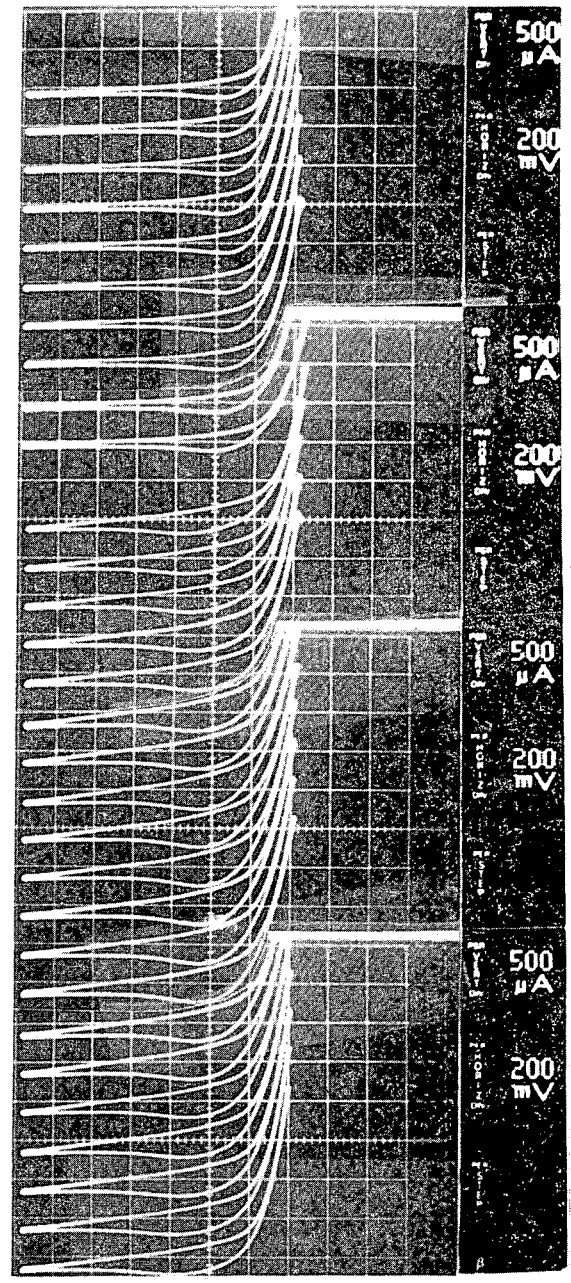

b. Left edge and grid No. 11 cleared

Fig. 4 Individual Au Grid Line Characteristics for Cell No. 653

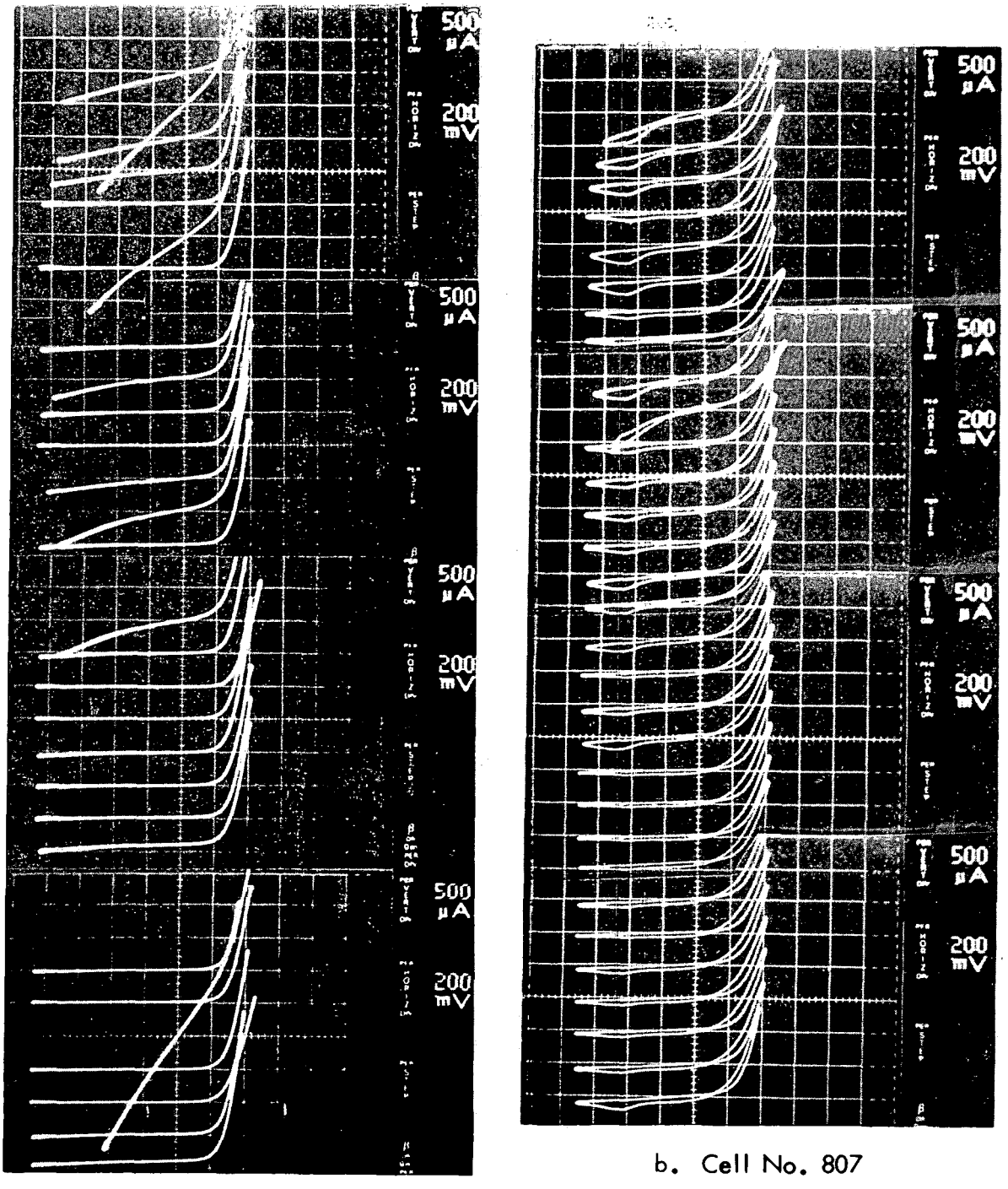

a. Cell No. 804

b. Cell No. 807

Fig. 5 Individual Au Grid Line Characteristics for Cu_2S/CdS/CdS:In Cells With High Resistivity Cu_2S

- All Au grid line diode characteristics similar (Fig. 5b). This is now a typical observation as a result of improved substrate cleaning and handling procedures

Localized areas of a device may be isolated by scribing the film surface. This was done on the device shown in Fig. 4. The remaining area (grids No. 12 through 31 interconnected) gave the large area cell characteristic presented in Fig. 1. Similarly, small areas of a device may be isolated for detailed I-V and/or C-V measurements.

The following measurement procedure has been adopted for the current stage of cell development:

(1) I-V characteristics of individual Au grid lines
(2) Interconnect (good) lines with Au bus bar
(3) Isolate small device area ($\sim 10^{-2}$ cm^2) for C-V and I-V diagnostic measurements
(4) Track development of large area solar cell characteristics from as-deposited state through various heat treatments with development of small area C-V and I-V characteristics

2.3 CdS CHARACTERIZATION

A representative review of the results of sputter deposition as applied to the Cu_2S/CdS cell is given in Table 3. With allowance made for the relative effort expended to date on the various process combinations given in Table 3, it is evident that the main problem is with material properties of the sputtered CdS layer.

Early in this study of CdS and $Cd_{.9}Zn_{.1}S$ deposition by reactive sputtering, it became evident that some features of the sputter deposition process were qualitatively different from the high rate, single source, vacuum evaporation process. The bottom line result is that conductivity control by a stoichiometric excess of Cd is difficult by the sputtering process. Theoretical considerations relevant to sputter deposition of a

Table 3

Cu_2S/CdS CELL DEPOSITION PROCESSES AND EFFICIENCIES OBTAINED

		Cu_2S			
		Conventional (a)		Sputtered (b)	
CdS	Conventional	IEC [1] Westinghouse [2] U. of Stuttgart [3]	≈ 9% ≈ 6% ≈ 7%	LLL [4] Annamalai [5]	≈ 4% < 2%
	Sputtered (b)	Leybold-Heraeus [6] Efremenkova, et al. [7] R. Hill [8]	≈.8% < 1% < 1%	Leybold-Heraeus [6] LMSC/Telic [9] LLL [10]	≈ 1% ≈ .6% < 1%

(a) Includes both wet dip and dry barrier processes

(b) Includes inert gas and reactive sputtering both with and without magnetic plasma confinement

[1] J. D. Meakin et al., Institute of Energy Conversion, Final Report on Contract EG-77-C-03-1536 (May, 1979)

[2] J. R. Szedon et al., Westinghouse R&D Center, Final Report on Contract DE-AC03-77 ET20429 (July, 1979)

[3] W. Arnolt et al., 2nd E. C. Photovoltaic Solar Energy Conference, ed. by R. VanOverstraeten, and W. Palz, D. Reidel Publ. Co., Dordrecht (1979), pp 826 – 842

[4] G. A. Armantrout, Lawrence Livermore Laboratory, Tech. Status Report 1/1/77 – 6/30/78 on Contract W-7405-Eng-48 (Jan 1979)

[5] N. K. Annamalai, 12th IEEE Photovoltaic Specialists Conference, 1976, pp 547 – 548

[6] W. Muller et al., Thin Solid Films 59, 327 (1979)

[7] V. M. Efremenkova et al., Izv. Acad. Nauk. SSSR, Ser. Fiz. 32, 1242 (1968)

[8] R. Hill, Newcastle upon Tyne Polytechnic, private communication (Jan 1980)

[9] W. W. Anderson, Contractors Indepth Review Meeting, SERI (Dec 1979)

[10] G. A. Armantrout and L. D. Partain, Contractors Indepth Review Meeting, SERI (Feb 1979)

compound, both constituents of which are separately quite volatile at the substrate temperatures of interest, were given in Reference 1.

The slow film deposition rate via the sputtering process ($R \approx 1-2$ μm/h at substrate temperatures $T_s \sim 250-300$ C) allows the growing film to more nearly approach its thermal equilibrium state. Vacuum evaporation deposition is normally carried out at a much higher rate, $R \approx 1-2$ μm/min (Ref. 15) and with an excess of Cd in the vapor stream (Ref. 5). An artifically high Cd flux can be introduced in the sputtered vapor stream by reducing the H_2S partial pressure cyclically or in the steady state. By cyclically sputtering Cd in Ar/H_2S and Ar, CdS films with $\rho \approx 10^3$ Ω-cm were obtained. (This deposition process was used to prepare Cells 653 and 654. See Fig. 1 and Tables 1 and 2.)

An alternative to deviation from stoichiometry resistivity control is impurity doping. Considerable experience with In as a dopant is available from the early Clevite work (Ref. 5). Cells with 6% conversion efficiency were produced. There is a high degree of dopant distribution control available in the reactive sputter deposition process. Of particular interest and importance is the ability to change dopant and/or alloy composition during deposition by switching cathodes. The SEM cross section shown in Fig. 3 is a composite of 0.5-μm undoped CdS on top of 7.0 μm of 1.0% In-doped CdS. Note that there is no discernible discontinuity in the columnar grain structure when the deposition cathodes were switched. The electrical characteristics of this composite CdS layer are described in the following section in relation to device characteristics.

Section 3
DEVICE-MATERIAL PARAMETER CHARACTERIZATION

The all-sputtered Cu_2S/CdS cell is a very planar structure as shown by the visibility of the interference fringes for both the CdS layer ($V_{CdS} \approx 0.10$) and the Cu_2S layer ($V_{Cu_2S} \approx 0.13$) as shown in Fig. 6. The strong CdS interference, still visible with the Cu_2S overlayer, provides a convenient nondestructive measurement of CdS layer thickness.

When the back surface reflectivity specific to Nb from Fig. 6 is introduced into the solar cell quantum efficiency Eq. (1)

$$\eta = \frac{\alpha L_n}{\alpha^2 L_n^2 - 1}\left[\frac{\alpha L_n\left(1 - R e^{-2\alpha t}\right) - (1 + R) e^{-\alpha t} \sinh \frac{t}{L_n}}{\cosh \frac{t}{L_n}} + \alpha L_n e^{-\alpha t} (R - 1)\right] \quad (1)$$

and integrated over the solar spectrum, we find the predicted maximum short circuit current densities of Fig. 7 as a function of Cu_2S layer thickness. Also shown in Fig. 7 are the photocurrent densities previously calculated for perfectly reflecting and nonreflecting back surfaces (Ref. 1). Note that the nonideal ($R \neq 1$) reflectively of Nb only reduces J_L by 7 to 11% depending on L_n compared to a reduction of 21 to 28% for a completely nonreflecting ($R = 0$) back wall.

No correction for multiple pass interference is included in Eq. (1). However, significant interference is observed in Fig. 6. Hill and coworkers (Ref. 16) have shown that interference phenomena in planar cells can be used to significantly enhance cell response.

The spectral response of a cell is shown in Fig. 8. For comparison, the shape of the spectral response calculated from Eq. (1) is shown for the indicated parameters.

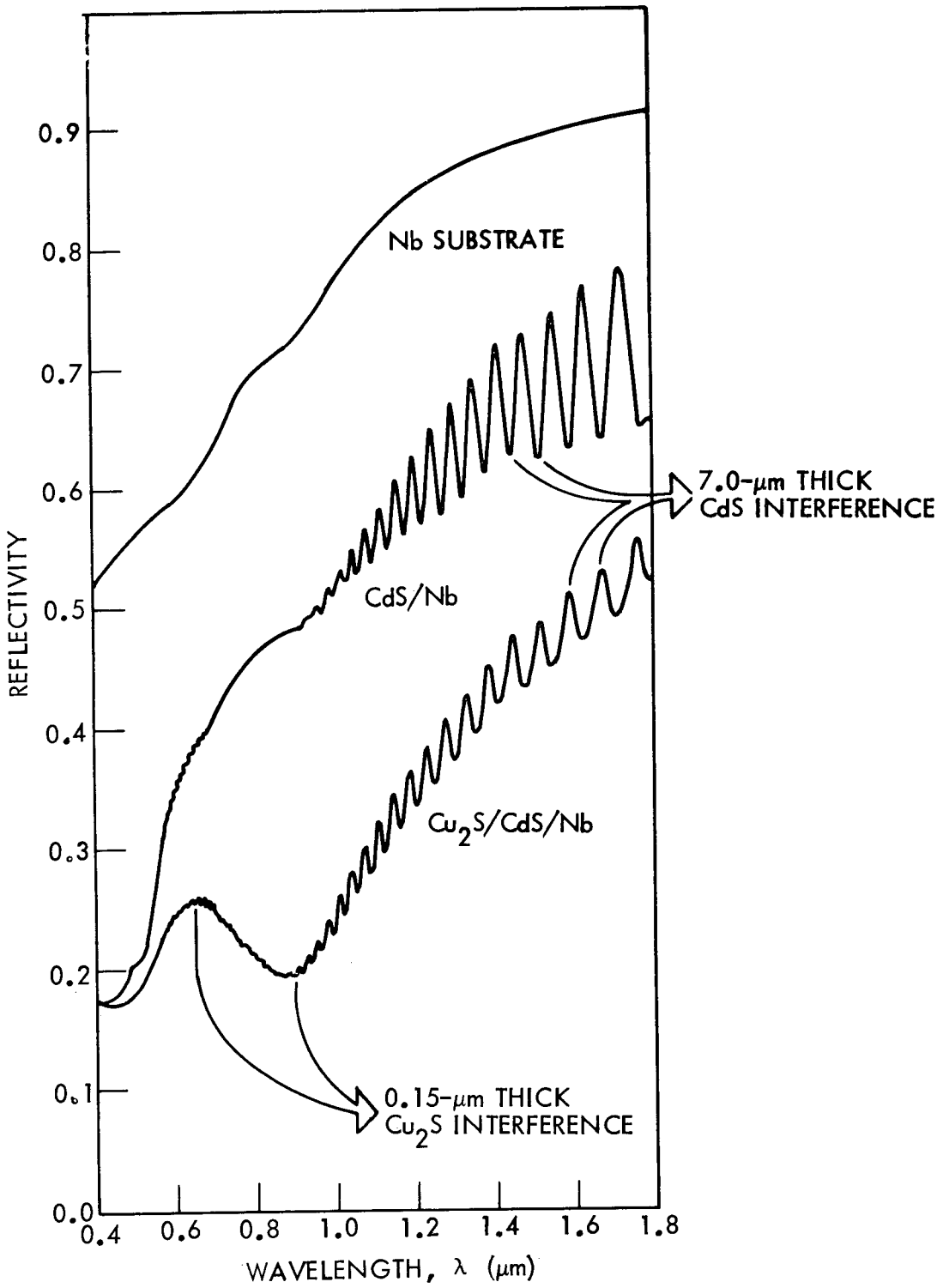

Fig. 6 Spectral Reflectivity of Successive Layers of Cu_2S/CdS/Nb Solar Cell Structure

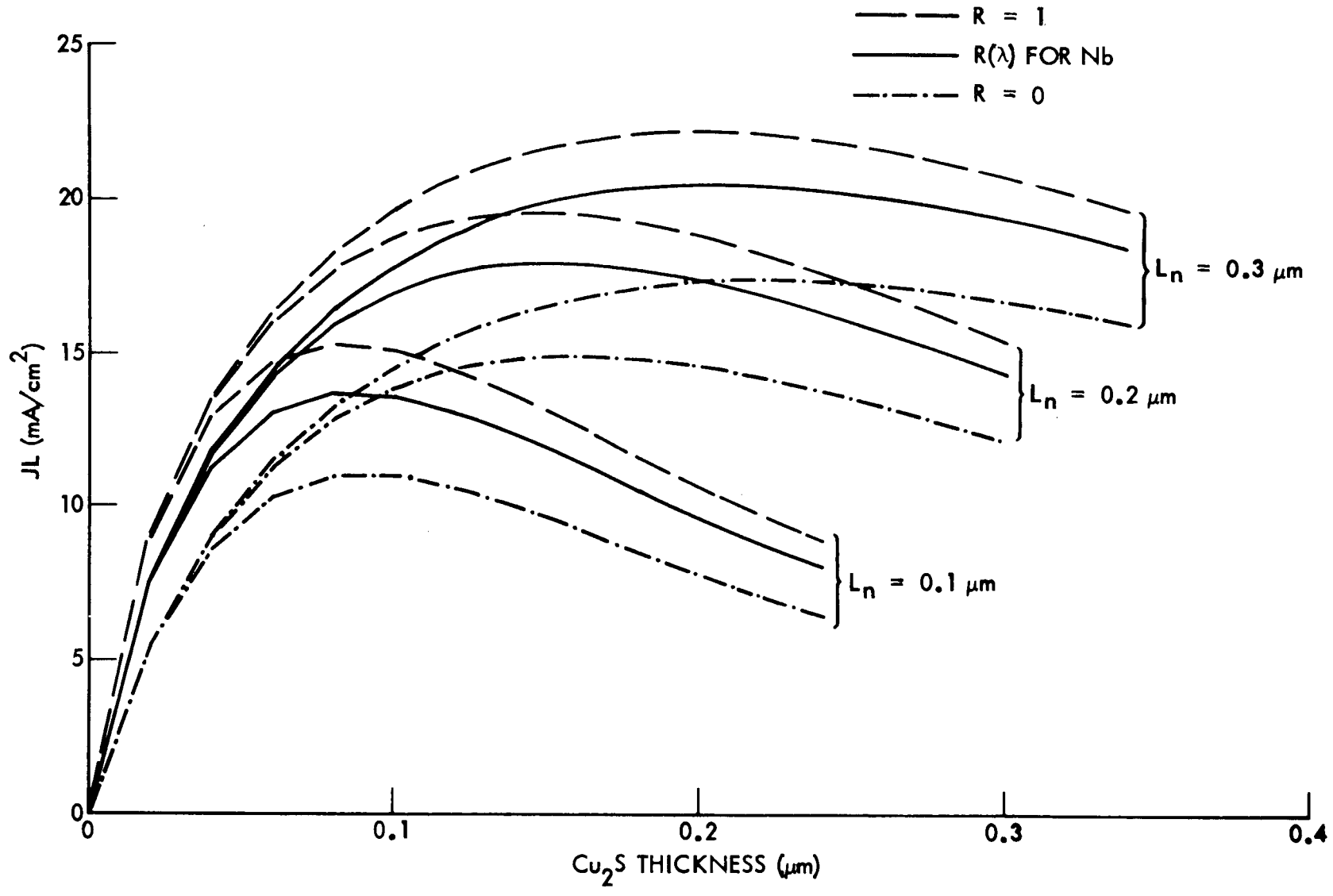

Fig. 7 Maximum Short Circuit Current Obtainable From Cu_2S Layer With Back Surface Reflectivity and Minority Carrier Lifetime as Parameters

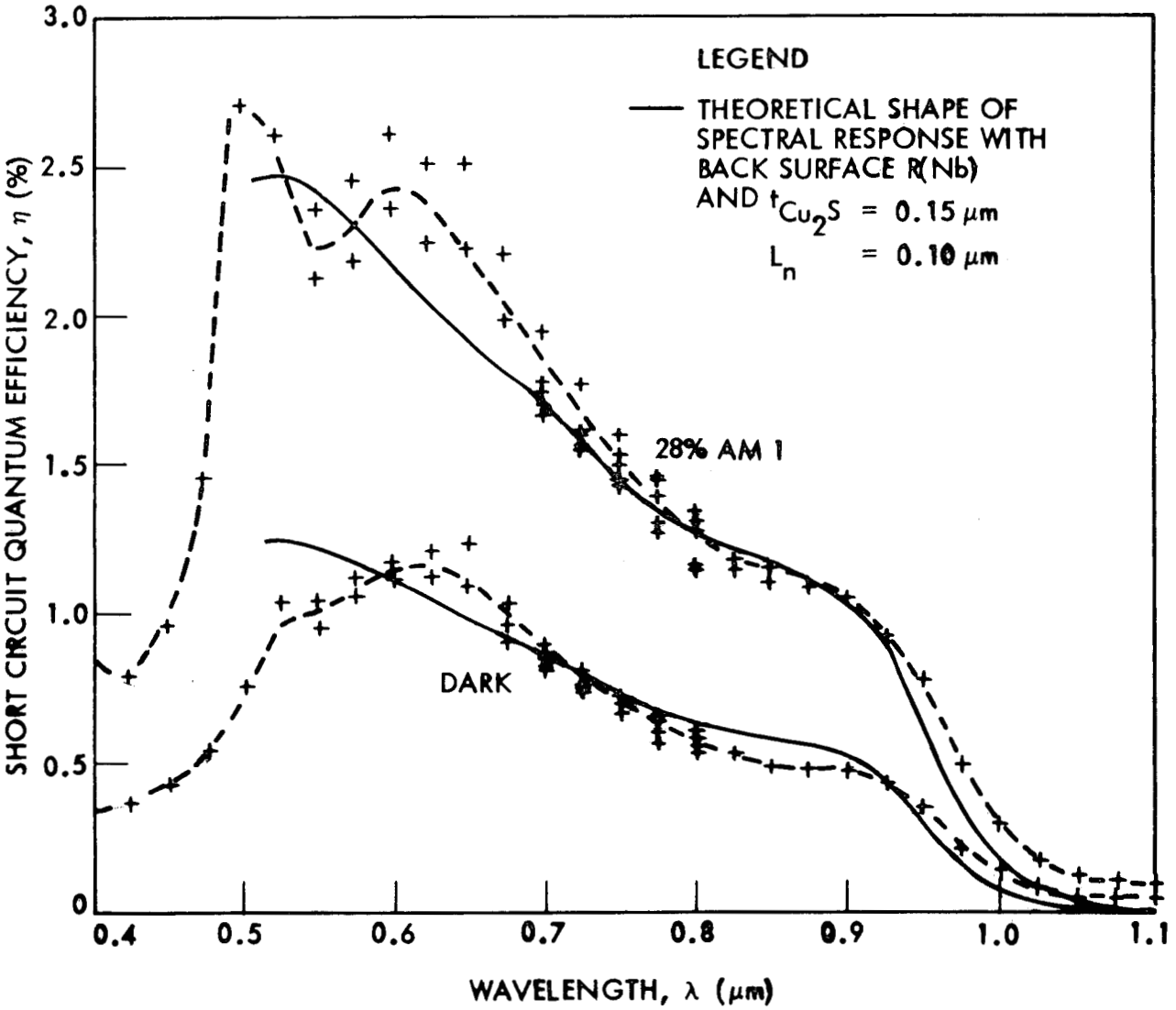

Fig. 8 Spectral Response of All Sputter Deposited CdS/Cu_2S Cell No. 824

The calculation does not include multiple pass interference. Nevertheless, reasonable agreement is obtained for $0.51 < \lambda < 1.0$ μm. The dip in short-circuit current on the long/wavelength side of the CdS absorption edge was noted in early Cu_2S/CdS cell studies and recently studied by Robertson and Woods (Ref. 17).

The conclusions to be drawn from Figs. 7 and 8 and Table 2 are:

- Observed photo current is generated in the Cu_2S layer.
- Junction carrier collection efficiency is, $\eta_j < 0.15$ to 0.25, depending on L_n when $J_{SC} \approx 3$ mA/cm^2

Rothwarf's theory of field aided junction collection efficiency (Ref. 6) predicts:

$$\eta_j = \frac{E_o}{\frac{S_j}{\mu} + E_o} \tag{2}$$

where, for a uniform effective donor dopant density, N_D^*, in the CdS adjacent to the junction,

$$E_o = \sqrt{\frac{2\, q\, N_D^* (V_D - V)}{\epsilon_r \epsilon_o}} \tag{3}$$

where V_D is the diffusion potential in the CdS and V is the nonequilibrium or external junction voltage.

For the low collection efficiency of all sputtered junctions to date,

$$S_j/\mu \gg E_o$$

and

$$\eta_j \approx \frac{\mu}{S_j}\sqrt{\frac{2\,q\,N_D^*\,V_D}{\epsilon_r\,\epsilon_o}}\left(1-\frac{V}{V_D}\right)^{1/2} \tag{4}$$

which implies a nonsaturating reverse bias photocurrent until $E_o \approx (S_j)/\mu$. A linear relation between I^2 and V implied by Eq. (4) is commonly observed as shown for two cells in Fig. 9. The plot for Cell 653 is only taken to -0.3 V since an incipient reverse breakdown occurs at V ≈ 0.4 V under AM 1 as may be seen from Fig. 1. While complete data were not taken on the cells examined to date to evaluate all of the quantities in Eq. (4) [or Eq. (2)], we estimate $2.4 \times 10^4 > S_j/\mu > 3.87 \times 10^3$ V/cm for Cell 653 and $7.8 \times 10^3 > S_j/\mu > 4.6 \times 10^3$ V/cm for cell 917. These numbers were based on N_D^*s obtained from van der Pauw measurements on CdS similar to that used in Cell 653 and the observed series resistance of the cell. C-V measurements under AM 1 illumination were used to determine N_D^* on cell 917. Junction efficiency was taken to be $J_{sc}/15.5$ which underestimates η_j. (See Tables 1 and 2.) These values of S_j/μ are comparable to those observed in good cells $S_j/\mu \approx 1.37 \times 10^3 - 4.48 \times 10^3$ V/cm from Ref. (18) . However, the interface electric field intensity is much too low.

To obtain low CdS bulk resistivity and maintain a high interface collection field, multilayer CdS/CdS:In structures are being examined. The undoped or high resistivity CdS region is ~0.1- to 0.5-μm thick. Cells were deposited with 1.0%-at. In so that when the space charge layer expanded through the undoped CdS region, the heavily doped CdS region prevented further space charge layer widening under reverse bias. The predicted C-V behavior was observed as shown in Fig. 10. This cell was deposited with a 0.5-μm-thick undoped CdS region which agrees with the observed saturation of space charge layer width at W ≈ 0.48 μm. For a stepwise variation in doping, the functional form of E_o versus V changes from that given in Eq. (3) for uniform doping

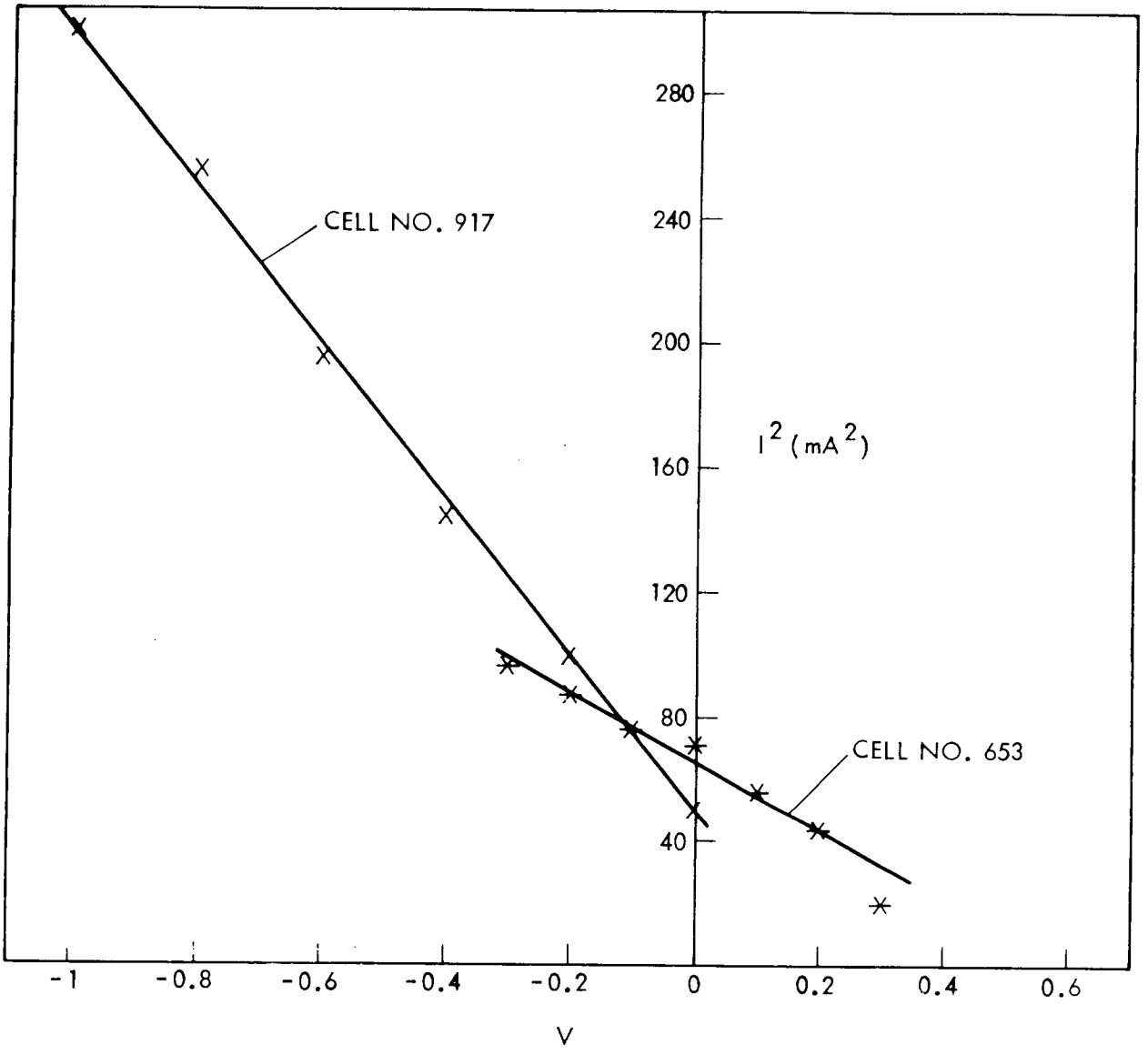

Fig. 9 Collected Photocurrent Squared Versus Device Voltage Under AM1 Illumination for Two Cells

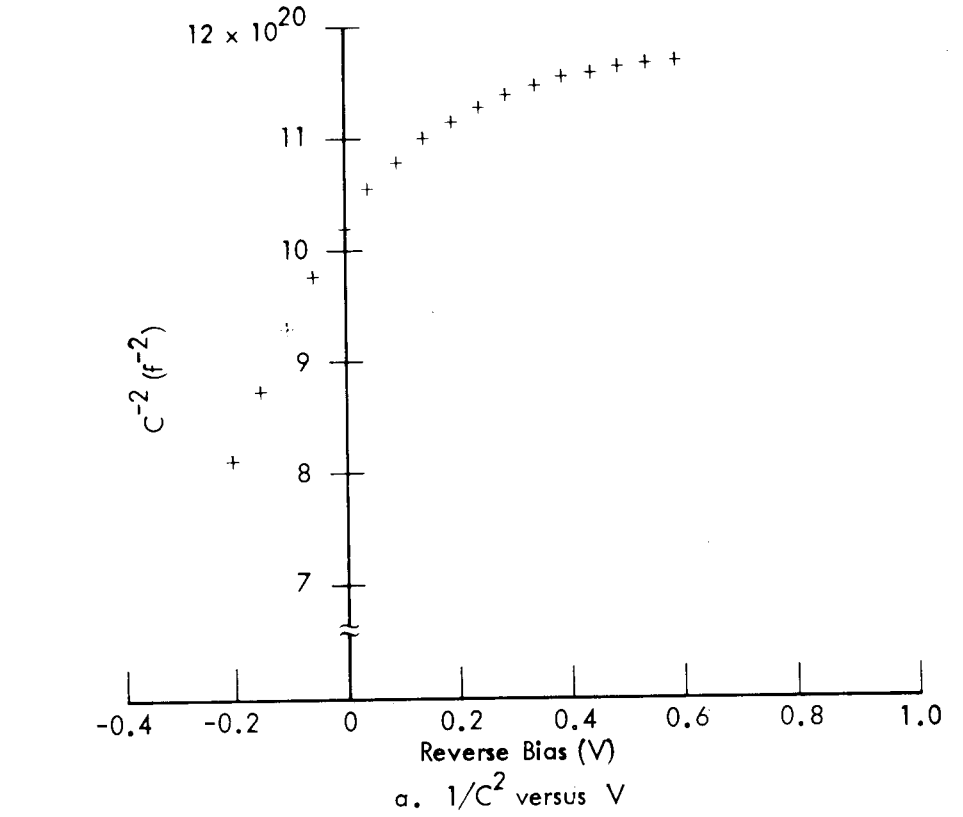

a. $1/C^2$ versus V

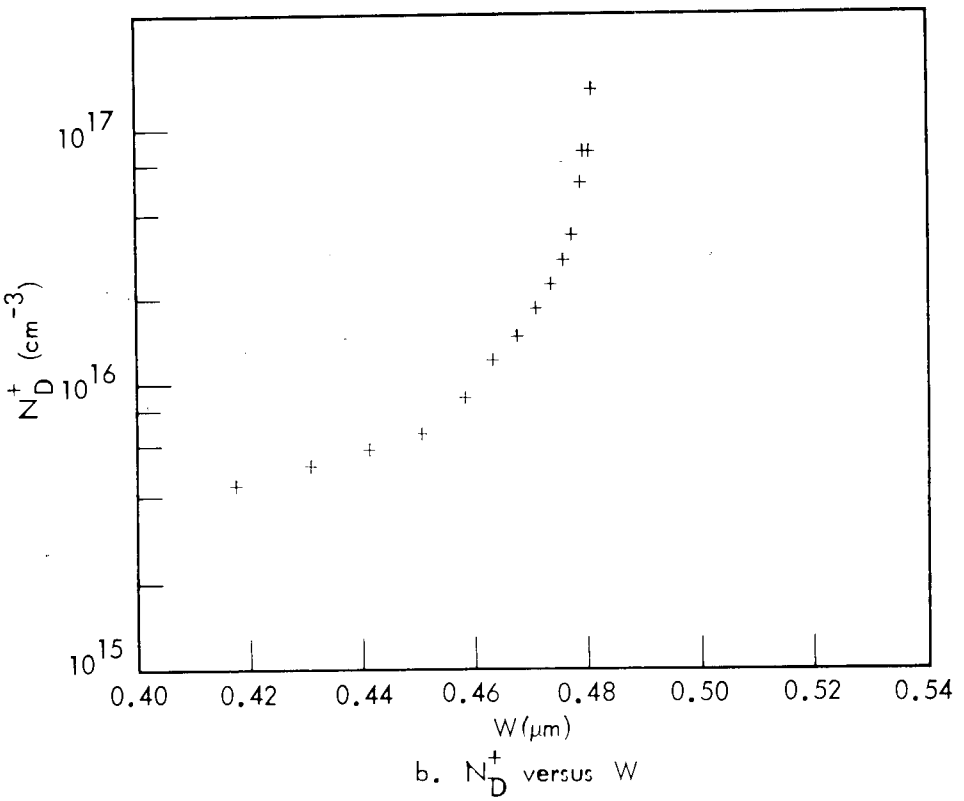

b. N_D^+ versus W

Fig. 10 Capacitance-Voltage and Corresponding Ionized Impurity Concentration Versus Depth for $Cu_2S/CdS/CdS:In$ Solar Cell Structure

to:

$$E_o = \frac{2 V_D}{W_1}\left(1 - \frac{V}{V_D}\right)^{1/2} \qquad \text{for } V \geq V_D\left(1 - \frac{W_0^2}{W_1^2}\right)$$

$$= \frac{W_0}{W_1^2} V_D \left(2\frac{W_0}{W_1} - 1\right) + \frac{V_D}{W_0}\left(1 - \frac{V}{V_D}\right) \text{for } V \leq V_D\left(1 - \frac{W_0^2}{W_1^2}\right)$$

where $W_1 \equiv \sqrt{\frac{2 \epsilon_r \epsilon_o V_D}{q N_D^*}}$ and W_o is the width of the lightly doped region.

The I-V characteristic of a solar cell with a doping level discontinuity is shown in Fig. 11. Note the linear I-V characteristic under AM1 illumination for $V < -0.1$ V under AM1 illumination.

For In-doped CdS and composite or multilayer structures, the effects of heat treatment during junction activation are expected to be different from conventional cells. Shiozawa et al. mentioned the different Cu diffusion, solubility, and photoconductivity for In-doped cells vis-á-vis undoped cells (Ref. 5). We have observed a great variability in heat treatment effects on our cells to date. Fig. 12 shows the development of cell characteristics similar to that described by TeVelde (Ref. 19). However, some cells rapidly develop a very high resistance during heat treatment. This was the case of Cell 917 described previously.

Finally, we note that, under forward bias, the I-V characteristics of the Cu_2S/CdS cells appear to be described by a TFL space charge-limited current flow (Ref. 3) as shown in Fig. 13 rather than the conventional diode equation. This type of I-V characteristic has also been observed on conventionally fabricated Cu_2S/CdS (Ref. 20). It has also been observed in other pn-heterojunctions (Ref. 21). The two different fabrication processes referred to in Fig. 13 are the off-stoichiometry doping of Cell 653 (see also Figs. 1 and 9) and the composite CdS structure of Cell 804 (see Fig. 10).

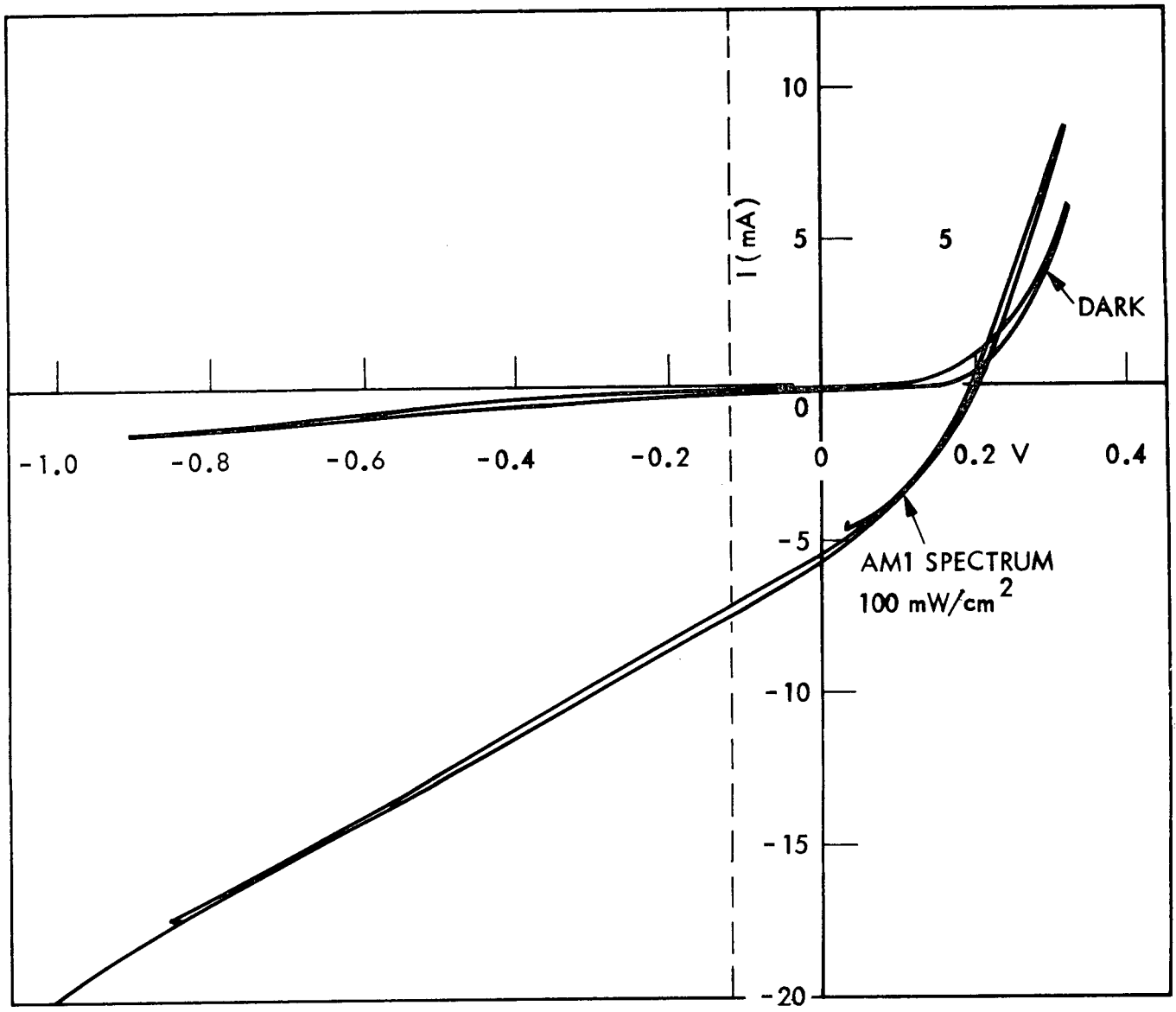

Fig. 11 I-V Characteristic of Cell No. 914 Which Shows Linear I-V Relation for $V < -0.1$

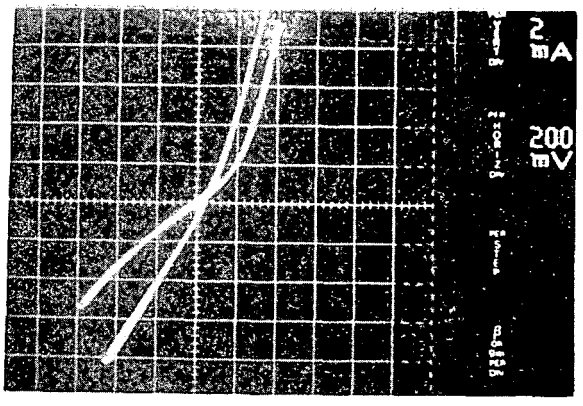

a. Unannealed

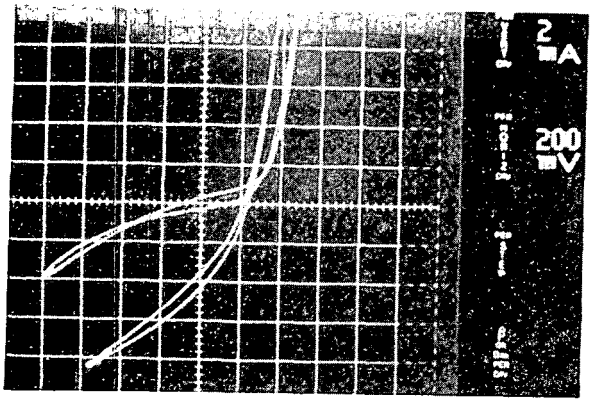

b. 2 min at 190°C

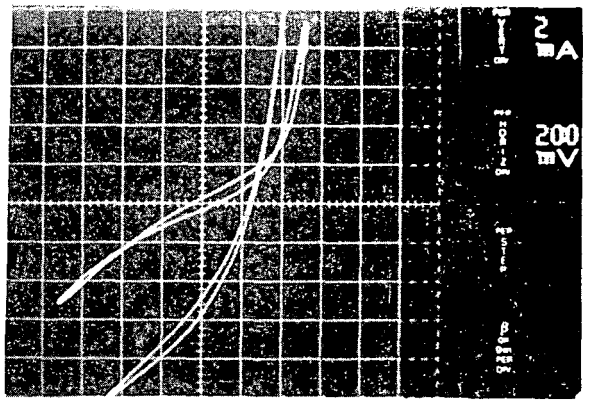

c. 4 min at 190°C

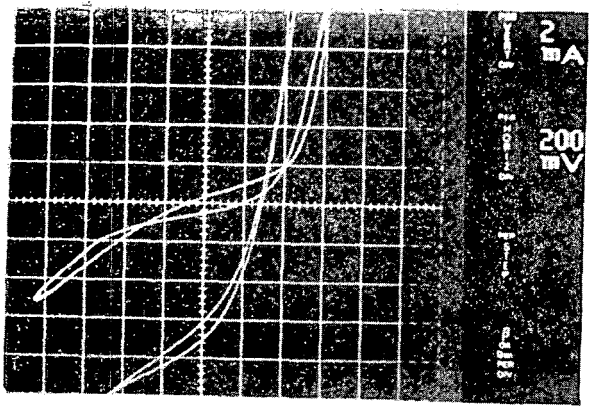

d. 6 min at 190°C

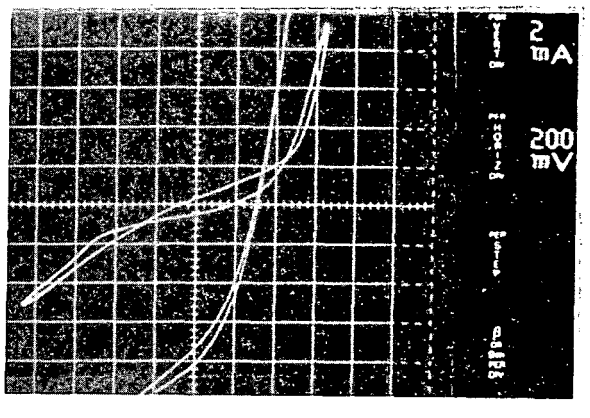

e. 8 min at 190°C

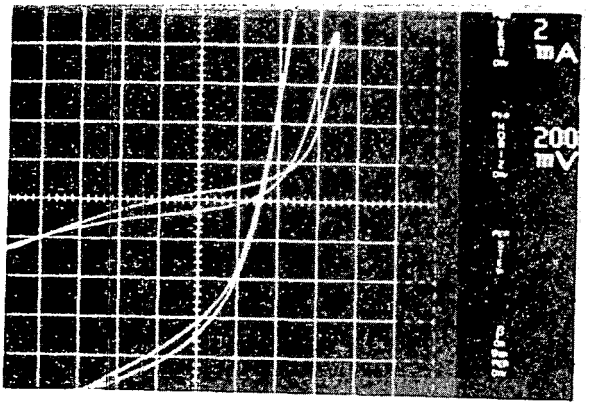

f. 10 min at 190°C

Fig. 12 Development of Dark and AM1 I-V Characteristic With Annealing at 190°C in H_2. Cell No. 824

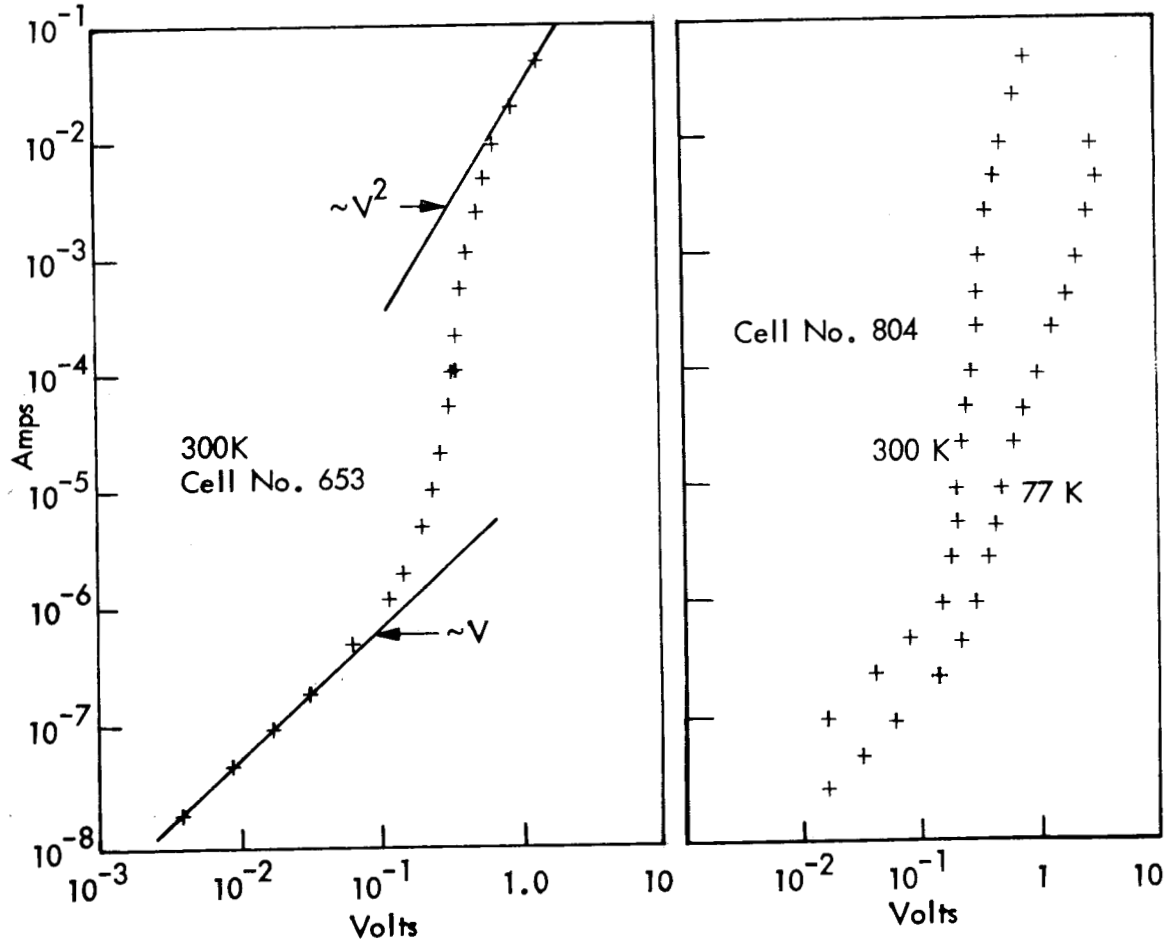

a. Cu_2S/CdS With Cyclic H_2S During CdS Sputtering

b. Cu_2S/CdS/CdS:In

Fig. 13 Current-Voltage Characteristics of Cu_2S/CdS Cells With Cds Deposited by Two Different Processes

Section 4

SUMMARY PLANS

Further work on an all-sputtered cell using a doped-CdS layer is based on the following three observations:

- Cu_2S with the required optoelectronic properties has been deposited by sputtering (this work and Refs. 22 and 23).
- The early Clevite program demonstrated In-doped CdS cells with 6-percent conversion efficiency (Ref. 5).
- Sputtering provides good control over electrical properties of In-doped CdS (this work).

Doped-cell structures to be investigated are described in terms of the CdS side of the junction:

- Uniform 0.1% In-doped CdS (comparable doping to Clevite cells)
- Composite CdS/1% In in CdS (preliminary results show promising results on interfacial field control)
- Composite CdS/0.1% In in CdS (minimize In content of cell)

The key issues to be evaluated with respect to the field-enhanced collection across the Cu_2S/CdS interface of the above cell structures are:

- Interface recombination velocity, S_j, in an all-sputtered heterojunction
- Cu diffusion in In-doped CdS
- Photoconductivity of Cu compensated In-doped CdS

These key issues determine the ability to reach a high (~1) junction collection efficiency. It is known that Cu diffusion and photoelectronic properties are different in In-doped and native defect-doped CdS. The fortuitous character of Cu diffusion and photoelectronic properties are essential to the efficient operation of conventional, native defect doped

CdS cells. It is necessary to carry out a new optimization procedure with In-doped CdS. A great deal of flexibility and control of impurity distribution in CdS is available from the sputtering deposition process used in this program.

As discussed in the preceding section, the AM1 illuminated I-V characteristic is dominated by the voltage dependence of the junction collection efficiency. Reduction of S_j/μ and/or increase of E_o will cause an improvement in device I-V characteristics. The quantities in Eq. (4) may be determined by C-V measurements under AM1 illumination and by η versus C measurements (Ref. 18). These quantities, in turn, are determined by the distribution of impurities and defects in the CdS. At this point, we have no quantitative information on the interdiffusion of elemental cell constituents during deposition or during heat treatment steps. A rational approach to J_{sc} and FF improvement will require the following set of measurements to be made as a function of deposition conditions and/or heat treatment:

- Development of AM1 J-V characteristics per Fig. 12
- Development of AM1 C-V characteristics, i.e., Fig. 10, repeated at each stage of cell processing
- Initial distribution and redistribution of Cu, In, and Cd during each stage of cell processing measured by SIMS or AES

Interfacial field control will be obtained by programmed deposition of CdS, CdS:In, Cd, etc. The efficacy of this approach was demonstrated during the current program (see Fig. 10). However, unexpected changes in device characteristics have occurred during heat treatment which are believed to be due to impurity diffusion. This requires qualitative confirmation and quantitative measurement before sensible corrective measures may be taken.

Section 5

REFERENCES

1. W. W. Anderson, A. D. Jonath, and J. A. Thornton, Cadmium Sulfide/Copper Sulfide Heterojunction Cell Research LMSC Final Report on Contract EG-77-C-03-1459 (Nov 1978)

2. A. Rothwarf, International Workshop on Cadmium Sulfide Solar Cells and Other Abrupt Heterojunctions, NSF-RANN AER 75-15858, University of Delaware, May 1975, pp 9 - 50

3. M. A. Lampert and P. Mark, Current Injection in Solids, Academic Press, New York, N. Y. 1970

4. J. Dieleman, International Workshop on Cadmium Sulfide Solar Cells and Other Abrupt Heterojunctions, NSF-RANN AER 75-15858, University of Delaware, May 1975, pp 92-107

5. L. R. Shiozawa, F. Augustine, G. A. Sullivan, J. M. Smith III and W. R. Cook, Jr., "Research on the Mechanism of the Photovoltaic Effect in High-Efficiency CdS Thin-Film Solar Cells", Contract AF33(615)-5224, ARL 69-0155, Oct 1969

6. A. Rothwarf, 2nd E. C. Photovoltaic Solar Energy Conference, ed. R. Van Overstraeten and W. Palz, D. Reidel Publishing Co., Dordrecht, 1979, pp 370-378

7. F. Guastavino, Contribution a l'etude des Properties Electriques et Optiques des Sulfures de Cuivre Cu_xS dans le Domaine 1, 75 x 2, 00 Thesis, Universite des Sciences et Techniques du Languedoc, Mar 1974

8. Lockheed Missile and Space Company, Inc., Cadmium Sulfide/Copper Sulfide Heterojunction Research, Technical Progress Report 3, Contract EG-77-C-03-1459 LMSC-D626523, Jun 1978

9. A. D. Jonath, W. W. Anderson, J. A. Thornton, and D. G. Cornog, J. Vac. Science and Technology 16, 200,1979

10. B. J. Mulder, Phys. Status Solidi (a) 13, 79, 1972

11. J. A. Thornton, Cadmium Sulfide/Copper Sulfide Heterojunction Cell Research Telic Corp. Tech. Progress Report 2, Contract XJ-9-8033-2, Nov 1979

12. W. W. Anderson, CdS/Cu_2S and CdS/Cu-Ternary Compound Program Contractors In-Depth Review Meeting, SERI, Wheatridge, CO, Dec 1979

13. C. A. Mead and W. G. Spitzer, Phys. Rev., 134, A713, 1964

14. D. L. Losee and E. L. Wolf, Phys. Rev. 187, 925, 1969

15. J. D. Meakin, et al. Cadmium Sulfide/Copper Sulfide Heterojunction Cell Research, Final Report on Contract EG-77-C-03-1576, May 1979

16. B. Gandham, R. Hill, H. A. Macleod and M. Bowden, Photovoltaic Solar Energy Conference, D. Reidel Publ. Co., Dordrecht, 1977, pp 1121-1130

17. M. J. Robertson and J. Woods, 2nd E. C. Photovoltaic Solar Energy Conference, ed. R. Van Overstraeten and W. Palz., D. Reidel Publ. Co., 1979, pp 909-916

18. N. C. Wyeth and A. Rothwarf, J. Vac. Sci. Technol. 16, 1402, 1979

19. T. S. TeVelde, Solid-State Electronics 16, 1305, 1973

20. L. D. Partain, G. A. Armantrout, J. Leong and P. Warter, Space-Charge-Limited Current in Cu_xS/CdS Solar Cells, Lawrence Livermore Laboratory Preprint UCRL-82883, 22 Jun 1979

21. J. W. Balch and W. W. Anderson, Physica Status Solidi (a) 9, 567, 1972

22. G. A. Armantrout, Lawerence Livermore Laboratory, Technical Status Report 1/1/77 - 6/30/78 on Contract W-7405-Eng-48, Jan 1979

23. N. K. Annamalai, 12th IEEE Photovoltaic Specialists Conference, 1976, pp 547-548